

THE SLIM-DISK STATE OF THE ULTRALUMINOUS X-RAY SOURCE IN M83

ROBERTO SORIA

International Centre for Radio Astronomy Research, Curtin University, GPO Box U1987, Perth, WA 6845, Australia

K. D. KUNTZ

The Henry A. Rowland Department of Physics and Astronomy, Johns Hopkins University, 3400 N. Charles Street, Baltimore, MD 21218, USA

KNOX S. LONG

Space Telescope Science Institute, 3700 San Martin Drive, Baltimore, MD 21218, USA

WILLIAM P. BLAIR

The Henry A. Rowland Department of Physics and Astronomy, Johns Hopkins University, 3400 N. Charles Street, Baltimore, MD 21218, USA

PAUL P. PLUCINSKY

Harvard-Smithsonian Center for Astrophysics, 60 Garden Street, Cambridge, MA 02138, USA

AND

P. FRANK WINKLER

Department of Physics, Middlebury College, Middlebury, VT 05753, USA

To appear in ApJ

ABSTRACT

The transient ULX in M83 that went into outburst in or shortly before 2010 is still active. Our new *XMM-Newton* spectra show that it has a curved spectrum typical of the upper end of the high/soft state or slim-disk state. It appears to be spanning the gap between Galactic stellar-mass black holes and the ultraluminous state, at X-ray luminosities $\approx 1\text{--}3 \times 10^{39}$ erg s^{−1} (a factor of two lower than in the 2010–2011 *Chandra* observations). From its broadened disk-like spectral shape at that luminosity, and from the fitted inner-disk radius and temperature, we argue that the accreting object is an ordinary stellar-mass black hole with $M \sim 10\text{--}20 M_{\odot}$. We suggest that in the 2010–2011 *Chandra* observations, the source was seen at a higher accretion rate, resulting in a power-law-dominated spectrum with a soft excess at large radii.

Keywords: accretion, accretion disks — black hole physics — galaxies: individual (M83) — X-rays: binaries

1. INTRODUCTION

The most luminous sub-class of X-ray binaries is known as ultraluminous X-ray sources (ULXs). They are a heterogeneous class of objects, empirically defined as non-nuclear accreting systems with an X-ray luminosity $L_X \gtrsim 3 \times 10^{39}$ erg s^{−1} (Feng & Soria 2011 for a review). As such, ULXs are more luminous than ordinary stellar-mass black holes (BHs) in our own Galaxy, which typically peak at $L_X \lesssim 10^{39}$ erg s^{−1}. The two main competing scenarios invoked to explain the bulk of the ULX population are higher BH masses and super-critical accretion. The mass of a BH determines its critical accretion rate and the corresponding Eddington luminosity. Galactic BHs have masses $\approx 10 M_{\odot}$ (Kreidberg et al. 2012) and a corresponding Eddington luminosity $L_{\text{Edd}} \approx 10^{39}$ erg s^{−1}; however, stellar evolution models predict that BHs with masses up to $\approx 80 M_{\odot}$ (Belczynski et al. 2010) may be formed via direct collapse of metal-poor stars of initial mass $> 120 M_{\odot}$. Alternatively, if the accre-

tion rate is super-critical ($\dot{m} \equiv 0.1 \dot{M} c^2 / L_{\text{Edd}} > 1$), the accretion luminosity may exceed the Eddington limit slightly: $L \approx L_{\text{Edd}}(1 + \ln \dot{m})$ for advection-dominated inflows, or $L \approx L_{\text{Edd}}(1 + \frac{3}{5} \ln \dot{m})$ when accretion is limited by radiatively-driven outflows (Poutanen et al. 2007; Shakura & Sunyaev 1973). Testing between the two alternative scenarios (more massive BHs or super-Eddington accretion) has proven challenging, owing to the scarcity of kinematic mass measurements for BHs in ULXs.

There are indirect methods for estimating BH masses in X-ray binaries, based on their spectral state behaviour (McClintock & Remillard 2006). At low or moderate accretion rates (low/hard state: $\dot{m} \lesssim$ a few percent), BH X-ray binaries are dominated by a hard power-law spectrum produced in a hot, geometrically thick, optically thin Comptonizing region; they are also radio-loud, that is they sustain a steady relativistic jet. At higher accretion rates (high/soft state: $\dot{m} \lesssim 0.5$) they are dominated by thermal emission from a geometrically thin, optically thick accretion disk, and the jet is quenched. Low/hard

and high/soft state are easily distinguished with X-ray and radio observations. The evolutionary track between the two states is also well modelled and fairly standard for all BH transients (Fender et al. 2004). Thus, the empirical identification of either state provides an order-of-magnitude estimate of the Eddington ratio and therefore of the BH mass. Moreover, when a BH X-ray binary is in the high/soft state, a more robust estimate of the BH mass comes from the fitted inner radius and peak temperature of the accretion disk, based on standard disk models and on the assumption that the disk extends down to the innermost stable circular orbit (Kubota et al. 1998; Shakura & Sunyaev 1973). For even higher accretion rates ($\dot{m} \gtrsim 0.5$), there is still no consensus about any direct relation between Eddington ratio and X-ray appearance. In the same range of observed luminosities, some ULXs appear power-law-dominated, others have a curved or thermal spectrum (Sutton et al. 2013; Soria 2011). There is also no consensus about the underlying physical evolution of the accretion flow when the accretion rate reaches Eddington. In one scenario, the inflow can still be described as a (non-standard) accretion disk (slim disk models: Watarai et al. 2001). Alternatively, many ULX X-ray spectra have been modelled with Comptonized emission from a warm ($kT \lesssim 2$ keV), optically thick medium (corona and/or dense outflow) which covers or replaces the inner disk (Gladstone et al. 2009; Done & Kubota 2006). Finally, it is still not clear whether power-law-like and curved ULX spectra correspond to different ranges of super-Eddington accretion rates, or instead to different viewing angles and outflow thickness (Sutton et al. 2013; Kawashima et al. 2012). In this context, discovering and monitoring transient ULXs is crucial to disentangle intrinsic changes in the inflow and emission properties from orientation effects.

1.1. Transient ULX in M83

In 2010, we detected a new ULX (Soria et al. 2012) in an inter-arm region of the spiral galaxy M83 [$d = (4.6 \pm 0.2)$ Mpc: Saha et al. 2006]. Located at R.A.(2000) = $13^{\text{h}}37^{\text{m}}05^{\text{s}}.13 \pm 0^{\text{s}}.01$, Dec.(2000) = $-29^{\circ}52'07''.1 \pm 0''.2$, it is listed as source X299 in our full *Chandra* catalog of M83 sources (Long et al. 2014). Henceforth, we will refer to this source as M83 ULX-1, for simplicity. Finding a ULX in M83 is remarkable in itself, given the unusually high metal abundance (up to twice the solar abundance) of the inner disk in this galaxy (Bresolin & Kennicutt 2002; Pilyugin et al. 2006, 2010). Solar-metallicity stars are not expected to produce BHs more massive than $\approx 15 M_{\odot}$ (Belczynski et al. 2010). Thus, the detection of M83 ULX-1 is already a strong argument in support of the interpretation of ULXs as super-Eddington sources rather than particularly heavy stellar BHs.

Although its luminosity is not extreme for a ULX ($L_{\text{X}} \approx 5 \times 10^{39}$ erg s $^{-1}$ in the *Chandra* observations of 2011 March, with a plausible peak at $L_{\text{X}} \approx 7 \times 10^{39}$ erg s $^{-1}$ in the *Swift* observations of 2011 February), M83 ULX-1 has the unusual property of being a transient. Most ULXs in nearby galaxies are variable (by a factor of a few) but remain persistently above $\sim 10^{39}$ erg s $^{-1}$. For example, almost all ULXs found by *Einstein* in the 1980s and *ROSAT* in the 1990s are still bright today. Instead, ULX-1 was undetected prior to 2010, with an upper limit

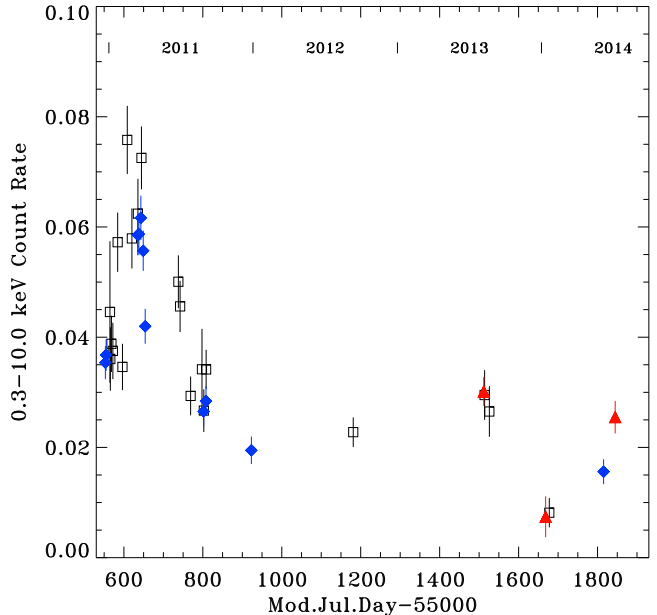


Figure 1. X-ray lightcurve from all our observations between 2010 December and 2014 July (Table 1), expressed as an equivalent *Swift*/XRT count rate. The flux in the *Chandra*/ACIS and *XMM-Newton*/EPIC observations was converted to a *Swift*/XRT count rate by convolving the best-fitting spectral models with an XRT response matrix. Black squares are the *Swift* datapoints; blue lozenges are those from *Chandra*; red triangles those from *XMM-Newton*.

$L_{\text{X}} \lesssim 2 \times 10^{37}$ erg s $^{-1}$ in *ROSAT* (1993 observation) and *XMM-Newton* (2003 observation), and $L_{\text{X}} \lesssim 10^{36}$ erg s $^{-1}$ in a 2000 *Chandra* observation (Soria et al. 2012). In Galactic BH X-ray binaries, transient systems usually contain low-mass evolved donors, while persistent systems have more massive Be stars or supergiants. We showed (Soria et al. 2012) that the donor of ULX-1 is indeed a relatively old star, probably a red giant with a mass $< 4 M_{\odot}$ and an age \gtrsim a few 100 Myr. The blue optical counterpart seen only during the outburst arises from a large X-ray-irradiated disk.

Because it is known to be a transient, it is plausible that ULX-1 will undergo state transitions analogous to those of transient stellar-mass BHs. If so, we can estimate its BH mass in two ways: a) by determining the luminosities at which the system transitions from the ultraluminous state to the canonical thermal dominant (high/soft) state, and then from the thermal dominant state to the low/hard state; and b) by fitting the disk parameters (temperature and innermost radius) while the source is in the thermal dominant state. Therefore, we have continued to monitor this source in an attempt to understand the intrinsic nature of ULXs and the connection between ULXs and Galactic BH X-ray binaries.

2. NEW X-RAY OBSERVATIONS OF M83 ULX-1

Since our extensive multiband 2010–2011 campaign (Long et al. 2014), we have carried out a number of X-ray observations of M83 (Table 1). Specifically, we used the *Swift* X-Ray Telescope (XRT) to carry out short (≈ 2 –5 ks) observations on 2012 September 11, 2013 August 9 and 21, and 2014 January 20. In addition, we used the

EPIC cameras on board *XMM-Newton* to observe the ULX on 2013 August 7 (≈ 50 ks), 2014 January 11 (≈ 40 ks) and 2014 July 6 (≈ 30 ks). Finally, in the analysis reported here, we make use of a 30-ks *Chandra*/ACIS-I observation of M83 which took place on 2014 June 7, which PI Ann Hornschemeier has kindly made available to us.

The *Swift* light curve (Figure 1) was produced from the standard level-2 data products. In all cases, the ULX was placed at the aim point, so that the response and the point spread function are well characterized. The count rates in the various bands were extracted as described by Soria et al. (2012). Because the *Swift* monitoring data had rather short exposures, the number of counts is insufficient for spectral fitting, and determining the absolute flux is problematic. To avoid these issues, the light curve is expressed in *Swift*/XRT 0.3–10.0 keV count rates. We then placed observations from other missions (with much higher total counts per observation) onto this scale by fitting those spectra and applying the latest *Swift*/XRT response to the best-fit models. The hardness ratio (Figure 2) was expressed as the ratio of *Swift*/XRT count rates in the 2.0–10.0 keV band over that in the 0.3–2.0 keV band, and the measurements from the other missions were similarly placed on the *Swift*/XRT scale. Since Soria et al. (2012), the *Swift*/XRT responses appropriate for 2011 have been changed significantly and the light curve has been updated accordingly. However, the overall response is not thought to have changed drastically in the 2011–2014 period over which these data were taken.

We processed the *XMM-Newton*/EPIC Observation Data Files with the Science Analysis System (SAS) version 13.0.0 (xmmas201300501). The particle background was low during all three observations, so we did not need to filter out any exposure interval. We defined a circular source extraction region centered on the ULX, with a $20''$ radius, sufficiently small to avoid significant contamination from the nuclear starburst emission. We extracted the background from a composite region three times as large, suitably selected at the same distance from the galactic nucleus, and not including any other bright sources or chip gaps. We selected single and double events (pattern ≤ 4 for the pn and pattern ≤ 12 for MOS1 and MOS2), with the standard flagging criteria `#XMMEA_EP` and `#XMMEA_EM` for the pn and MOS, respectively. After building response and ancillary response files with the SAS tasks *rmfgen* and *arfgen*, we used *epicspeccombine* to create average EPIC spectra and response files for each of the three epochs. Finally, we grouped the spectra to a minimum of 20 counts per bin, so that we could use Gaussian statistics. We used XSPEC version 12.6 for spectral fitting (Arnaud 1996). For each epoch, we fitted the combined EPIC spectra, and we also fitted the three EPIC cameras simultaneously (leaving a free normalization factor between pn and MOS). The results from the two methods are always consistent within the 90% confidence limit, and the relative normalization factor between MOS and pn is ≈ 0.98 . In Table 2, we report the fit parameters for the combined EPIC spectra. For timing analysis, we used standard FTOOLS tasks (Blackburn 1995). Unlike most of the *Chandra*/ACIS-S spectra from 2010–2011, the *XMM-Newton*/EPIC spectra are not piled up (as shown by the SAS task *epatplot*).

We filtered and analyzed the *Chandra*/ACIS-I data

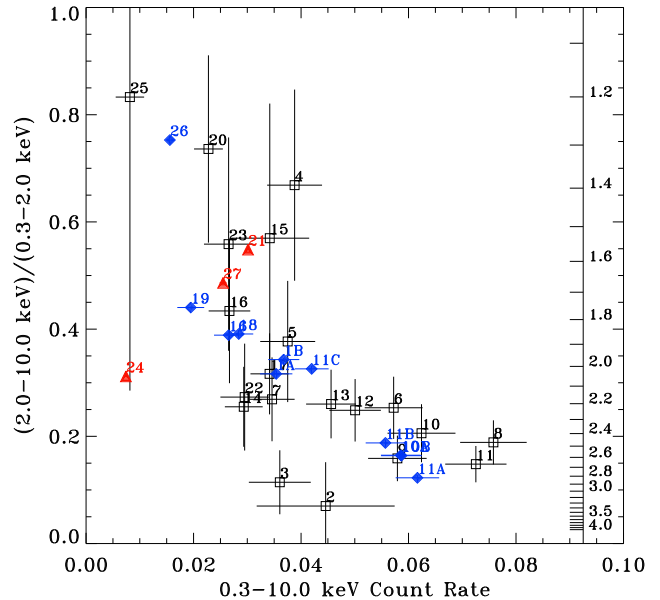


Figure 2. Hardness ratio as a function of *Swift*/XRT count rate. All hardness ratios have been converted to an equivalent *Swift*/XRT ratio of (2–10) keV/(0.3–2) keV count rates. The equivalent single-component power-law index is shown on the right. As in Figure 1, black squares are the *Swift* datapoints; blue lozenges are those from *Chandra*; red triangles those from *XMM-Newton*. Numbers refer to the sequential order of the observations (Table 1).

with standard imaging and spectroscopic tasks (*e.g.*, *dmcopy*, *dmextract*, and *specextract*), in the CIAO Version 4.6 (Fruscione et al. 2006) data analysis system. We used *PIMMS* Version 4.6b from the *Chandra* proposal planning toolkit to estimate the level of pile-up given the observed count rate, and found that it is $\approx 7\%$.

3. X-RAY FLUX AND HARDNESS RATIO

The 0.3–10 keV light curve suggests that the outburst peaked in February and March 2011, when it displayed strong week-to-week variability of as much as factors of two in flux. The flux declined steadily, with smaller week-to-week variability through the end of 2011 (Soria et al. 2012). Our new observations show that the decline did not continue significantly past the end of 2011. Eight measurements in the intervening years show that ULX-1 has maintained a roughly constant maximum flux, though with significant variations. Thus, although the source sometimes fades to below the ULX threshold, as it did in January 2014, the bulk of our measurements since 2011 have caught the source at $\sim 2 \times 10^{39}$ erg s $^{-1}$.

The hardness ratio shown in Figure 2 is the *Swift*/XRT count rate in the 2–10 keV band divided by the count rate at 0.3–2 keV. In general, the hardness ratio declines with flux, so that at higher luminosities the source is softer than at lower luminosities. The *Chandra* observations in 2010–2011 made it clear that a trend in hardness ratio was driven primarily by the fraction of the emission in the thermal disk (the greater the fraction the softer the overall emission) with some modification by the index of the power law. Most of the more recent data follow the same trend in the hardness-ratio vs count-rate diagram. The clear exception is the *XMM-Newton* measurement

Table 1
M83 X-ray Observations

Epoch	Obsid	Instrument	Date	Exposure (s)	Flux ^a (10^{-12} erg cm $^{-2}$ s $^{-1}$)	L_X^b (10^{39} erg s $^{-1}$)
<i>Swift</i>						
2	0031905002	XRT	2011-01-03	399	1.1 ± 0.3	
3	0031905003	XRT	2011-01-04	1620	1.0 ± 0.2	
4	0031905004	XRT	2011-01-07	2213	1.9 ± 0.3	
5	0031905005	XRT	2011-01-11	2140	1.4 ± 0.2	
6	0031905006	XRT	2011-01-23	2896	1.8 ± 0.2	
7	0031905007	XRT	2011-02-04	2938	1.1 ± 0.1	
8	0031905008	XRT	2011-02-16	2882	2.2 ± 0.2	
9	0031905009	XRT	2011-02-28	2863	1.6 ± 0.2	
10 ^c	0031905010	XRT	2011-03-15	2285	1.9 ± 0.2	
11 ^d	0031905011	XRT	2011-03-24	3258	2.0 ± 0.2	
12	0031905012	XRT	2011-06-25	3240	1.6 ± 0.2	
13	0031905013	XRT	2011-06-30	3146	1.5 ± 0.2	
14	0031905014	XRT	2011-07-27	3588	0.9 ± 0.1	
15	0031905015	XRT	2011-08-24	951	1.6 ± 0.3	
16 ^e	0031905016	XRT	2011-08-29	2706	1.1 ± 0.2	
17	0031905017	XRT	2011-09-04	4048	1.2 ± 0.1	
20	0031905018	XRT	2012-09-11	4882	1.2 ± 0.1	
22	0080498001	XRT	2013-08-09	2187	1.0 ± 0.1	
23	0080498002	XRT	2013-08-21	1915	1.2 ± 0.1	
25	0080498003	XRT	2014-01-20	2020	0.5 ± 0.2	
<i>Chandra</i>						
1A	12995	ACIS-S	2010-12-23	59291	1.2 ± 0.1	$3.6^{+0.2}_{-0.2}$
1B	13202	ACIS-S	2010-12-25	98780	1.3 ± 0.1	$4.4^{+0.5}_{-0.4}$
10A ^c	12993	ACIS-S	2011-03-15	49398	1.5 ± 0.1	$4.5^{+0.7}_{-0.3}$
10B	13241	ACIS-S	2011-03-18	78963	1.6 ± 0.1	$5.3^{+1.3}_{-0.7}$
11A ^d	12994	ACIS-S	2011-03-23	150058	1.6 ± 0.1	$5.1^{+0.5}_{-0.4}$
11B	12996	ACIS-S	2011-03-29	53044	1.5 ± 0.1	$5.3^{+1.1}_{-0.6}$
11C	13248	ACIS-S	2011-04-03	54329	1.5 ± 0.1	$5.0^{+1.0}_{-0.5}$
16 ^e	14332	ACIS-S	2011-08-29	52381	1.0 ± 0.1	$2.9^{+0.4}_{-0.4}$
18	12992	ACIS-S	2011-09-05	66286	1.0 ± 0.1	$3.2^{+0.5}_{-0.5}$
19	14342	ACIS-S	2011-12-28	67103	0.8 ± 0.1	$2.3^{+0.3}_{-0.2}$
26	16024	ACIS-I	2014-06-07	29588	0.7 ± 0.1	$2.0^{+0.2}_{-0.1}$
<i>XMM-Newton</i>						
21	0723450101	MOS1 MOS2 PN	2013-08-07	50143 49041 41666	1.15 ± 0.02	$3.4^{+0.3}_{-0.2}$
24	0723450201	MOS1 MOS2 PN	2014-01-11	43060 42164 24922	0.20 ± 0.01	$0.57^{+0.42}_{-0.03}$
27	0729561201	MOS1 MOS2 PN	2014-07-06	27448 27546 22904	0.87 ± 0.02	$2.5^{+0.2}_{-0.2}$

^a Observed flux in the 0.3–10 keV band.

^b Unabsorbed luminosity in the 0.3–10 keV band, calculated only for observations for which we have modelled the spectrum. For the *Chandra* observations, we adopted the luminosities published for the best-fitting *diskbb+pow* model, while for the *XMM-Newton* observations we used the *diskpbb* model.

^c The *Swift* exposure covered the first part of the *Chandra* exposure; the *Swift* exposure lasted from 12:17:32 to 22:05:56 while the *Chandra* exposure began at 12:21:40.

^d The *Swift* exposure covered the end of the *Chandra* exposure; the *Swift* exposure lasted from 11:20:06 to 21:05:57 while the *Chandra* exposure ended at 22:18:33.

^e The *Swift* and *Chandra* exposures were not quite coincident; the *Swift* exposure lasted from 11:35:00 to 15:13:56 while the *Chandra* exposure began at 18:41:51.

in January 2014 (epoch 24) when the source was exceptionally faint and the hardness ratio was soft rather than hard. To interpret this possible state transition, we will do a full spectral analysis of this observation, and compare it with the other two *XMM-Newton* observations. The *Swift* observation made slightly more than a week later (epoch 25) has a sufficiently large uncertainty that its hardness ratio could be consisted with either the low *XMM-Newton* observation or the previously noted trend.

It is very rare for transient Galactic stellar-mass BHs to be in outburst for such a long period of time, ≈ 4 years¹. The exception is GRS1915+105 which has been in outburst at luminosities $\approx 10^{39}$ erg s⁻¹ for over 20 years (Castro-Tirado et al. 1994). A few others among the most luminous Galactic BHs with a low-mass donor have shown long outbursts: ≈ 2 years for 4U 1630–47 (Tomsick et al. 2005); ≈ 1 year for GRO J1655–40 (Sobczak et al. 1999) and XTE J1550–564 (Sobczak et al. 2000). The outburst profile, with its initial peak, decline and reflarings, is also at least qualitatively similar to the outbursts of those three Galactic BHs.

4. X-RAY SPECTRAL STATE

To better understand the outburst evolution, we carried out spectral fits to the *XMM-Newton* data. The first question we asked was whether the spectra are consistent with a straight power-law, or are significantly curved. There is still no consensus on a definition of “canonical” ULX spectral states, but it has been clear from the earliest studies that, as a zeroth order approximation, some ULXs are in a power-law-like state, others have a curved spectrum, and some switch between the two states (Kubota et al. 2001; Makishima 2007; Soria 2011). As shown in Table 2, we find that none of the three *XMM-Newton* spectra is well fitted with a simple absorbed power-law; all exhibit significant curvature. An exponentially cut-off power-law (*cutoffpl* model in XSPEC) is a phenomenological way of highlighting the high-energy curvature, and this model does indeed provide very good fits (Table 2). The slope (photon index) of the power-law below the exponential cut-off is $\Gamma \approx 0.8$, much too flat for any physically plausible model (*e.g.*, inverse-Compton or synchrotron emission) applicable to X-ray binaries in the low/hard state. It corresponds to a flux density $F_\nu \propto \nu^{0.2 \pm 0.1}$, which is more consistent with the “flat” part of an accretion disk just below the Wien cutoff (Shakura & Sunyaev 1973; Frank et al. 2002).

We then tried more physical models, suitable to luminous X-ray binaries. A disk-blackbody (Shakura & Sunyaev 1973; Mitsuda et al. 1984; Makishima et al. 1986) plus power-law is the standard model used in the literature for classifying the accretion state of X-ray binaries. This model provides good fits to all three epochs of *XMM-Newton* data (Table 2). However, while such models formally describe the data, it is important to examine whether the values of the best-fitting parameters are physically plausible or self-consistent. In the first and third epoch, we find inner-disk temperatures ≈ 1.5 keV, which are too high for a standard accretion disk around stellar-mass

BHs. In Galactic BHs, typical values of the inner-disk temperature in the disk-dominated high/soft state are $\lesssim 1.2$ keV (McClintock & Remillard 2006). Given its high luminosity, M83 ULX-1 might be (if anything) a little more massive than typical Galactic BHs, in which case its disk temperature should be even lower. Only the second epoch of our *XMM-Newton* spectra is consistent with a canonical high/soft state dominated by a standard disk-blackbody with $kT_{\text{in}} \approx 0.9$ keV.

Higher-than-expected disk color temperatures are observed in other ULXs (Stobbs et al. 2006; Roberts 2007), and have been interpreted in two ways (although the difference may be at least partly semantic). In one model (Watarai et al. 2001; Mizuno et al. 2001; Kubota & Makishima 2004; Isobe et al. 2012), the standard disk evolves into a slim disk when the accretion rate reaches a critical level and the luminosity approaches or mildly exceeds the Eddington limit. One of the observable properties that distinguish a slim disk from a standard disk is a flatter radial temperature profile ($T(R) \propto R^{-p}$, where $p \approx 0.5 - 0.6$ rather than $p = 0.75$ as in the standard disk case). Another one is non-negligible emission from inside the innermost stable circular orbit (Watarai et al. 2000; Mizuno et al. 2001; Kulkarni et al. 2011), which makes the inner disk radius appear smaller than in the standard case. The slim disk model predicts higher peak color temperature ($kT_{\text{in}} \approx 1.5 - 2$ keV), as the inner part of the disk becomes dominated by electron scattering and radiative emission becomes less efficient. Alternatively (Done & Kubota 2006; Gladstone et al. 2009; Sutton et al. 2014), the same near-Eddington regime can be modelled as a warm ($kT_e \approx 1.5 - 2$ keV), optically thick ($\tau \sim 10$) scattering corona covering or replacing the inner part of a standard disk. The observed spectrum is then a combination of a disk-blackbody from the uncovered (larger and cooler) outer disk plus a scattering component from the warm corona, with a downturn above 3 keV. Both scenarios have been applied not only to ULXs, but also to the highest luminosity phases of some Galactic BHs; for example, the peak of the outburst in XTE J1550–564 was successfully explained in the slim-disk framework (Kubota & Makishima 2004) as well as in the warm-corona scenario (Done & Kubota 2006). In some cases, a second Comptonization component, produced in a hotter ($kT_e > 10$ keV), thinner corona ($\tau \sim 1$) may also be present, and responsible for the power-law component.

In our XSPEC spectral analysis of M83 ULX-1, we used the *diskpbb* model as an approximation of the slim disk (Figures 3, 4). This is also known in the literature as a p-free disk, or extended multicolor disk (Isobe et al. 2012). We used the Comptonization model *diskir* (Gierliński et al. 2009) to reproduce the outer-disk plus warm-corona scenario. Both sets of models provide formally good fits (Table 2). Some of the parameters in the Comptonization model for the 2014 January spectrum are poorly constrained because there is little evidence of a straight power-law above the curved thermal component at high energies. In fact, adding a power-law component to the *diskpbb* model does not improve the fit.

There is little difference in the fit statistics between the interpretation of our new results as a slim-disk regime (or other similar types of modified disk), or as a standard-

¹ See for example the *Rossi X-ray Timing Explorer* All Sky Monitor lightcurves at <http://xte.mit.edu/asmlc/ASM.html>.

Table 2
Spectral fits to the *XMM-Newton*/EPIC spectra

Parameter	Value in 2013 Aug	Value in 2014 Jan	Value in 2014 Jul
Power law: <i>phabs*phabs*po</i>			
$n_{\text{H,int}}$ (10^{20} cm $^{-2}$)	$12.7^{+0.9}_{-0.9}$	$17.0^{+2.4}_{-2.2}$	$11.6^{+1.3}_{-1.3}$
Γ	$1.85^{+0.03}_{-0.03}$	$2.42^{+0.09}_{-0.09}$	$1.92^{+0.04}_{-0.04}$
N_{po} (10^{-4})	$2.57^{+0.08}_{-0.08}$	$0.81^{+0.07}_{-0.06}$	$2.06^{+0.10}_{-0.09}$
χ^2/dof	1.26 (840.2/663)	1.17 (302.96/258)	1.21 (497.54/410)
$f_{0.3-10\text{keV}}$ (10^{-13} erg cm $^{-2}$ s $^{-1}$)	$12.0^{+0.2}_{-0.2}$	$2.1^{+0.1}_{-0.1}$	$9.0^{+0.2}_{-0.2}$
$L_{0.3-10\text{keV}}$ (10^{39} erg s $^{-1}$)	$4.0^{+0.1}_{-0.1}$	$1.00^{+0.07}_{-0.07}$	$3.1^{+0.1}_{-0.1}$
Cutoff power law: <i>phabs*phabs*cutoffpl</i>			
$n_{\text{H,int}}$ (10^{20} cm $^{-2}$)	$0.4^{+1.4}_{-0.4}$	$1.4^{+4.3}_{-1.4}$	< 1.0
Γ	$0.76^{+0.12}_{-0.07}$	$0.89^{+0.41}_{-0.27}$	$0.83^{+0.07}_{-0.07}$
E_{efold} (keV)	$3.0^{+0.4}_{-0.3}$	$1.9^{+0.7}_{-0.3}$	$2.9^{+0.3}_{-0.3}$
N_{po} (10^{-4})	$2.38^{+0.07}_{-0.06}$	$0.85^{+0.08}_{-0.07}$	$1.98^{+0.08}_{-0.08}$
χ^2/dof	0.90 (597.99/662)	1.02 (262.63/257)	0.91 (372.04/409)
$f_{0.3-10}$ (10^{-13} erg cm $^{-2}$ s $^{-1}$)	$11.5^{+0.2}_{-0.2}$	$2.0^{+0.1}_{-0.1}$	$8.7^{+0.2}_{-0.2}$
$L_{0.3-10\text{keV}}$ (10^{39} erg s $^{-1}$)	$3.1^{+0.1}_{-0.1}$	$0.57^{+0.07}_{-0.03}$	$2.4^{+0.1}_{-0.1}$
Disk blackbody + power law: <i>phabs*phabs*(diskbb+po)</i>			
$n_{\text{H,int}}$ (10^{20} cm $^{-2}$)	$5.7^{+3.7}_{-3.1}$	$0.2^{+16.0}_{-0.2}$	$2.4^{+5.0}_{-2.4}$
kT_{in} (keV)	$1.58^{+0.13}_{-0.14}$	$0.87^{+0.26}_{-0.08}$	$1.42^{+0.16}_{-0.15}$
N_{dbb} (10^{-3})	$6.3^{+2.4}_{-1.4}$	$13.1^{+5.9}_{-9.7}$	$7.4^{+3.7}_{-2.4}$
Γ	$2.00^{+0.38}_{-0.28}$	$1.8^{+1.2}_{-0.6}$	$1.93^{+0.50}_{-0.33}$
N_{po} (10^{-5})	$9.6^{+2.4}_{-2.7}$	$1.1^{+4.2}_{-0.4}$	$6.0^{+3.1}_{-2.1}$
χ^2/dof	0.91 (598.15/661)	1.05 (268.21/256)	0.91 (372.17/408)
$f_{0.3-10}$ (10^{-13} erg cm $^{-2}$ s $^{-1}$)	$11.5^{+0.2}_{-0.2}$	$2.0^{+0.1}_{-0.1}$	$8.7^{+0.2}_{-0.2}$
$L_{0.3-10\text{keV}}$ (10^{39} erg s $^{-1}$)	$3.4^{+0.3}_{-0.2}$	$0.57^{+0.42}_{-0.03}$	$2.5^{+0.2}_{-0.2}$
Extended disk-blackbody: <i>phabs*phabs*diskpbb</i>			
$n_{\text{H,int}}$ (10^{20} cm $^{-2}$)	$2.9^{+1.4}_{-1.4}$	$5.0^{+4.5}_{-4.5}$	$0.8^{+2.1}_{-0.8}$
kT_{in} (keV)	$1.90^{+0.12}_{-0.11}$	$1.23^{+0.22}_{-0.16}$	$1.72^{+0.17}_{-0.12}$
p	$0.63^{+0.02}_{-0.02}$	$0.56^{+0.07}_{-0.05}$	$0.63^{+0.02}_{-0.03}$
N_{disk} (10^{-3})	$2.6^{+1.0}_{-0.8}$	$1.9^{+2.7}_{-1.2}$	$3.0^{+1.5}_{-1.2}$
χ^2/dof	0.90 (595.95/662)	1.03 (263.84/257)	0.91 (370.43/409)
$f_{0.3-10\text{keV}}$ (10^{-13} erg cm $^{-2}$ s $^{-1}$)	$11.5^{+0.2}_{-0.2}$	$2.0^{+0.1}_{-0.1}$	$8.6^{+0.2}_{-0.2}$
$L_{0.3-10\text{keV}}$ (10^{39} erg s $^{-1}$)	$3.2^{+0.1}_{-0.1}$	$0.63^{+0.02}_{-0.02}$	$2.4^{+0.1}_{-0.1}$
Irradiated Comptonized disk: <i>phabs*phabs*diskir</i>			
$n_{\text{H,int}}$ (10^{20} cm $^{-2}$)	$0.5^{+0.8}_{-1.2}$	$0.1^{+0.8}_{-0.1}$	< 0.8
kT_{in} (keV)	$0.56^{+0.19}_{-0.16}$	$0.59^{+0.06}_{-0.13}$	$0.39^{+0.20}_{-0.15}$
Γ	$1.46^{+0.06}_{-0.06}$	$1.29^{+0.21}_{-*}$	$1.48^{+0.06}_{-0.06}$
kT_e (keV)	$1.44^{+0.22}_{-0.17}$	> 8.3	$1.29^{+0.16}_{-0.16}$
L_c/L_d	$1.9^{+2.8}_{-0.5}$	$5.0^{+3.5}_{-2.0}$	$2.7^{+3.3}_{-1.5}$
N_{dbb} (10^{-3})	200^{+45}_{-15}	53^{+62}_{-23}	473^{+1450}_{-360}
χ^2/dof	0.91 (597.84/660)	1.03 (263.43/255)	0.91 (371.34/407)
$f_{0.3-10\text{keV}}$ (10^{-13} erg cm $^{-2}$ s $^{-1}$)	$11.5^{+0.2}_{-0.2}$	$2.0^{+0.1}_{-0.1}$	$8.6^{+0.2}_{-0.2}$
$L_{0.3-10\text{keV}}$ (10^{39} erg s $^{-1}$)	$3.1^{+0.1}_{-0.1}$	$0.56^{+0.03}_{-0.02}$	$2.3^{+0.1}_{-0.1}$

^a All errors are given at the 90% confidence level. In all cases, we assume a fixed Galactic column density $n_{\text{H}} = 4 \times 10^{20}$ cm $^{-2}$ in addition to a fitted intrinsic absorption column. Fluxes are observed values; luminosities are defined as $4\pi d^2 \times$ the unabsorbed flux. For the *diskir* model, we assumed $f_{\text{in}} = 0.1$, $r_{\text{irr}} = 1.2$, $f_{\text{out}} = 0.005$ and $\log r_{\text{out}} = 5.0$.

outer-disk plus warm, optically-thick Comptonized component; thus, we must look at the general evolution of the source from epoch to epoch to make a tentative choice between them. We had interpreted the 2010–2011 *Chandra*/ACIS spectra in the frame of a disk plus hot-corona model (Soria et al. 2012) because there is no evidence of a high-energy downturn or curvature above 2 keV in the *Chandra* spectra, which were mostly taken at higher luminosity phases of the outburst. For all those spectra, we can only place a lower limit to the coronal temperature, as $kT_e > 1.8$ keV at all epochs (Soria et al. 2012) and in one case (2011 March 15) $kT_e > 6.5$ keV. However, estimating or constraining a possible high-energy downturn in those spectra is difficult for at least two reasons: firstly, *Chandra*’s sensitivity above 5 keV is much lower than *XMM-Newton*’s; secondly, the *Chandra* spectra suffer from pile-up, which flattens the slope at high energies and may mask a downturn. Thus, we suggest now that ULX-1 was more dominated by Comptonization during the *Chandra* observations, but we cannot make any stronger inference on the temperature of the Comptonizing medium (see Section 6 for a more detailed discussion of the differences between the spectral states in the two sets of observations).

In the *XMM-Newton* spectra, instead, the high-energy curvature is significant, and corresponds to characteristic temperatures $kT \approx 1.5$ keV, 1.2 keV and 1.7 keV for the three epochs. Taking into account that these temperatures are relatively low for a Comptonizing corona, and that the second epoch is also consistent with a canonical high/soft state, we favour the slim-disk interpretation for these observations. We suggest that in 2013–2014, ULX-1 was at the boundary between the high/soft and slim disk states, varying between just below and just above the Eddington luminosity. The trend of increasing temperatures with flux suggests disk emission as the most plausible interpretation. For coronal emission, we would instead expect a decrease in temperatures with increasing flux, because the increased illumination would cool the corona (Middleton et al. 2011). The low value of $p \approx 0.6 < 0.75$ found in all three epochs indicates that the disk is always non-standard, including during the 2014 January observation, when the X-ray luminosity was $\approx 6 \times 10^{38}$ erg s $^{-1}$ (Table 2). Extensive studies of bright Galactic BH X-ray binaries show that deviations from the standard disk spectrum start to appear at disk luminosities $\sim 0.3L_{\text{Edd}}$ (Steiner et al. 2010). This suggests that the BH mass of M83 ULX-1 is $\lesssim 20M_{\odot}$. For a slim disk model, we would have expected p to decrease with luminosity, with $p \rightarrow 0.5$ at the highest fluxes; instead, the index is consistent with a constant value $p \approx 0.6$ at all three epochs. It is unclear how to interpret this finding. It is important to remember that X-ray spectral fits give us the scaling of the color temperature $T_{\text{col}} \propto R^{-p}$, with T_{col} related to the effective temperature T_{eff} by a hardening factor κ , that is $T_{\text{col}} \equiv \kappa T_{\text{eff}}$ (Shimura & Takahara 1995). A small dependence of κ on disk radius at the highest accretion rates would be sufficient to produce the observed small discrepancy from the underlying slim-disk relation $T_{\text{eff}} \propto R^{-0.5}$. Therefore, we do not think that the fitted values of p are a significant argument against a disk-dominated spectrum.

In terms of unabsorbed luminosities, regardless of the spectral model, ULX-1 was below the formal ULX

threshold in 2014 January, while it was in the ULX regime in the other two epochs, although a factor of 2 or 3 fainter than in early 2011. Note that, for simplicity, all luminosities listed in Table 2 are defined as $4\pi d^2 \times$ the unabsorbed flux (isotropic emission). Strictly speaking, this is a good approximation for the emission from a spherical or quasi-spherical inflow (*e.g.*, the power-law component), while for a standard thin disk, the luminosity is $2\pi d^2 (\cos \theta)^{-1} \times$ the flux, where θ is the (unknown) viewing angle. For the slim disk model, we also numerically calculated the isotropic bolometric luminosity in the three epochs: $L_{\text{bol}} = (3.7 \pm 0.1) \times 10^{39}$ erg s $^{-1}$ in 2013 August, $(9.2 \pm 0.2) \times 10^{38}$ erg s $^{-1}$ in 2014 January, and $(2.7 \pm 0.1) \times 10^{39}$ erg s $^{-1}$ in 2014 July. If our interpretation of ULX-1 as a source that is straddling the Eddington threshold is correct (see Section 5), these luminosities correspond to BH masses ~ 10 – $20M_{\odot}$, consistent with a normal stellar-mass BH.

5. BH MASS ESTIMATE

When disk emission dominates the spectrum of an accreting BH, it is possible to determine the physical inner disk radius R_{in} from the XSPEC model normalization N , provided that we can constrain two correction factors: the hardening factor κ for the observed color temperature, and a geometric factor ξ that depends on how close to the innermost stable circular orbit the disk reaches its peak temperature:

$$R_{\text{in}} \approx \xi \kappa^2 N^{1/2} (\cos \theta)^{-1/2} d_{10\text{kpc}} \text{ km} \quad (1)$$

(Kubota et al. 1998; Makishima et al. 2000). Then, from R_{in} we can estimate a characteristic BH mass, as a function of spin parameter: $R_{\text{in}} \approx \alpha GM_{\text{BH}}/c^2$, where $\alpha = 6$ for a non-rotating BH, $\alpha = 1$ for a maximally rotating Kerr BH, and $\alpha = 1.24$ for the maximum spin achievable by an astrophysical BH (spin parameter $a = 0.998$; Thorne 1974).

In the case of standard disks, $\xi \approx 0.412$ (Kubota et al. 1998) and $\kappa \approx 1.7$ (Shimura & Takahara 1995; Davis et al. 2005), so that $R_{\text{in}} \approx 1.19 \times 460 N^{1/2} (\cos \theta)^{-1/2}$ km at the adopted distance of M83. If we interpret the 2014 January spectrum as a canonical high/soft state, we obtain $R_{\text{in}} \approx 63_{-32}^{+15} (\cos \theta)^{-1/2}$ km (Table 2). This is consistent with a slowly-spinning $10M_{\odot}$ BH, or a maximally-spinning $60M_{\odot}$ BH.

However, this approximation holds only for luminosities $\lesssim 0.3L_{\text{Edd}}$. At higher accretion rates, the hardening factor κ increases with luminosity and can be as high as ≈ 2.5 – 3 for some Galactic BHs (*e.g.*, GRO J1655–40 at outburst peak, and GRS 1915+105) and for ULXs in the slim-disk state (Watarai & Mineshige 2003; Kawaguchi 2003; Shrader & Titarchuk 2003; Isobe et al. 2012). This is why at near-Eddington luminosities, the fitted color temperature T_{in} increases faster than the standard $T_{\text{in}} \propto L_{\text{disk}}^{1/4}$ high/soft state relation (“anomalous regime”: Kubota & Makishima 2004; Abe et al. 2005). Given the luminosities of M83 ULX-1 in the three *XMM-Newton* epochs, and the fact that a disk model with $p \approx 0.6$ provides the best fit to the data, we argue that the source was likely to be in the anomalous regime (slightly below Eddington) or in the slim disk regime (slightly above Eddington), and therefore

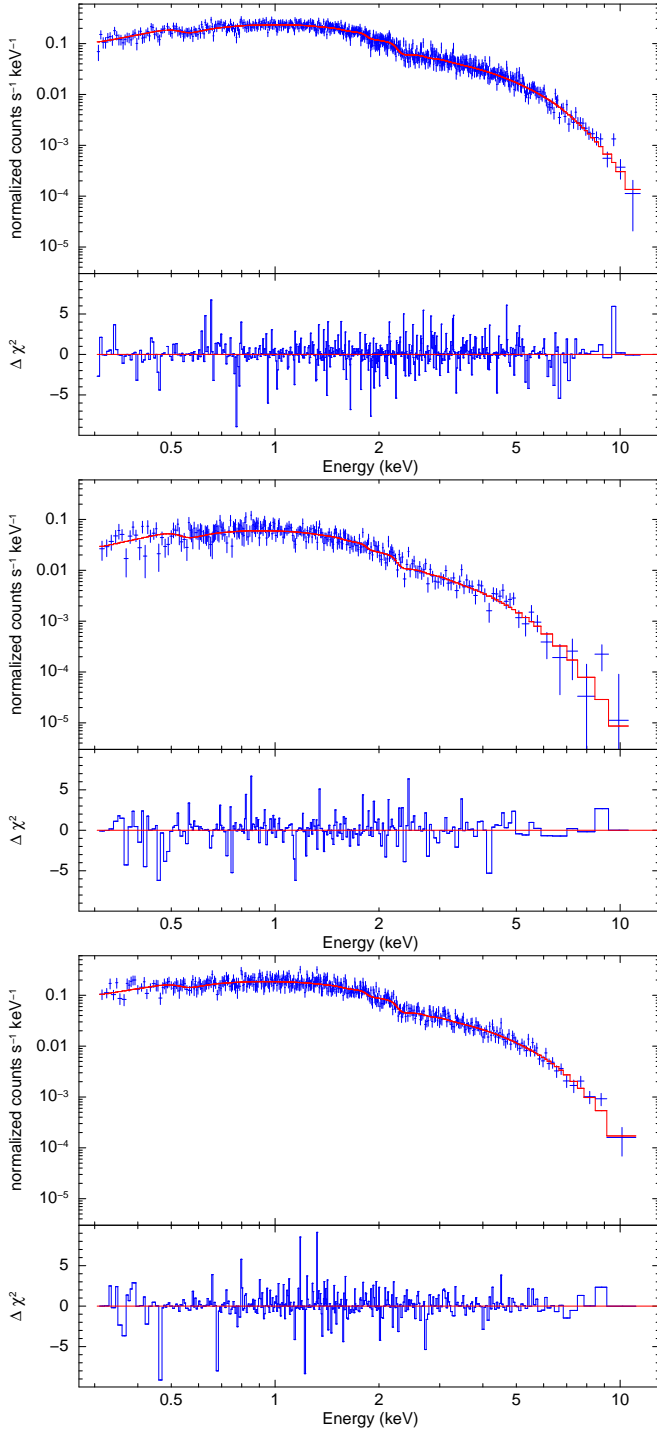


Figure 3. Top panel: *XMM-Newton*/EPIC spectrum and χ^2 residuals from the 2013 August observation, fitted with an extended (p-free) disk-blackbody model (*diskbb* in XSPEC). We show here the average EPIC spectrum obtained by combining pn and MOS spectral files with the SAS task *epicspecombine*. Middle panel: same, for the 2014 January observation. Bottom panel: same, for the 2014 July data. See Table 2 for the best-fitting parameters.

we take a hardening factor $\kappa \approx 3$ for BH mass estimates. Following Vierdayanti et al. (2008), we also take $\xi \approx 0.353$, which takes into account the transonic flow in the pseudo-Newtonian potential. Taking an average normalization constant $N_{\text{disk}} = (2.5 \pm 0.5) \times 10^{-3}$ from our *diskbb* fit (Table 2), we obtain a “true” inner disk

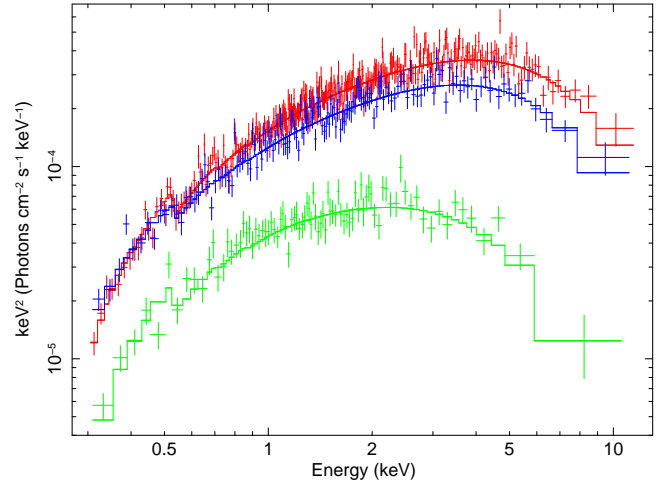


Figure 4. Unfolded *XMM-Newton*/EPIC spectra for all three epochs, fitted with the *diskbb* model in XSPEC; 2013 August = red; 2014 January = green; 2014 July = blue. The spectra have been rebinned to a minimum signal-to-noise ratio of 6 in each bin, for display purposes only. See Table 2 for the best-fitting parameters.

radius $R_{\text{in}} \approx (73 \pm 15)(\cos \theta)^{-1/2}$ km. This corresponds to an “apparent” BH mass

$$M_X = \left(\frac{6}{\alpha}\right) \left(\frac{\xi}{0.353}\right) \left(\frac{\kappa}{3}\right)^2 \frac{8.2 \pm 1.7}{(\cos \theta)^{1/2}} M_{\odot}. \quad (2)$$

Finally, we need to take into account that the inner radius of a slim disk extends slightly inside the innermost stable circular orbit, so that the true mass $M_{\text{BH}} \approx 1.2 M_X$ (Vierdayanti et al. 2008). This gives our final best estimate of the BH mass as

$$M_{\text{BH}} = \left(\frac{6}{\alpha}\right) \left(\frac{\xi}{0.353}\right) \left(\frac{\kappa}{3}\right)^2 \frac{10 \pm 2}{(\cos \theta)^{1/2}} M_{\odot}. \quad (3)$$

In principle, the estimated mass can be as high as $\approx 60 M_{\odot}$ in the (implausible) extreme Kerr scenario; however, the fact that the system appears to be in the anomalous regime (upper end of the high/soft state) or in the slim disk state for a moderate bolometric luminosity $\approx 2 \times 10^{39}$ erg s $^{-1}$ (and possibly even lower, considering the 2014 January spectrum) suggests that the BH mass is closer to ~ 10 – $20 M_{\odot}$. The same argument holds if we interpret the X-ray spectra as Comptonized emission from a warm, optically-thick corona, which is typical of sources at $L_X \approx 1$ – $3 L_{\text{Edd}}$ (Gladstone et al. 2009).

Our newly estimated BH mass ~ 10 – $20 M_{\odot}$ is less than the mass estimate proposed in Soria et al. (2012). In that study, we had not observed the source in a thermal state, which limited our ability to estimate the inner disk radius; moreover, in the absence of other constraints, we conservatively assumed that ULX-1 peaked at around its the Eddington limit. Instead, if our revised mass estimate is correct, ULX-1 must have peaked at $L_X \approx 3$ – $4 L_{\text{Edd}}$ during the 2010–2011 *Chandra* observations.

6. SUPER-EDDINGTON REGIME

Although the idea of moderately super-Eddington emission was somewhat frowned upon until recently, there is no strong theoretical argument against it: it is well known that above the critical accretion rate, $L \approx L_{\text{Edd}}(1 + a \ln \dot{m})$ where $0.6 \lesssim a \lesssim 1$ (Shakura & Sunyaev

1973; Poutanen et al. 2007; King 2014). Hence, the accretion rate required to produce $L_X \approx 3L_{\text{Edd}}$ is $\dot{m} \sim 10$ (regardless of BH mass). For a $15\text{-}M_\odot$ BH, with $L_{\text{Edd}} \approx 2 \times 10^{39} \text{ erg s}^{-1}$, $\dot{m} \sim 10$ corresponds to a physical accretion rate $\dot{M} \sim 3 \times 10^{-6} M_\odot \text{ yr}^{-1}$, which is a plausible value if the Roche-lobe-filling donor star is expanding along the red giant branch or undergoing asymptotic-giant-branch pulsations. Observationally, several recent studies have shown evidence of super-critical accretion and in some cases, mildly super-Eddington luminosity (Liu et al. 2013; Motch et al. 2014; Soria et al. 2014).

A more complicated and unsolved problem is determining when super-Eddington BHs have a thermal, curved X-ray spectrum (slim-disk or warm, optically-thick corona models) and when they have instead a power-law-dominated spectrum (consistent with an hotter, optically-thin corona). Some ULXs (*e.g.*, IC 342 X-1 and X-2: Kubota et al. 2001; NGC 1313 X-2: Grisé et al., in prep.) have been observed in a power-law-like state at lower luminosities, and in a curved-spectrum state at higher luminosities. However, other ULXs (*e.g.*, Holmberg IX X-1: Soria 2011 and references therein) have been observed to switch between power-law and curved spectra over a largely overlapping range of luminosities. M 83 ULX-1 was certainly brighter during the *Chandra* observations, when its spectrum was more power-law dominated without evidence of a high-energy downturn but with a soft excess at low temperatures ($kT \sim 0.2\text{--}0.4 \text{ keV}$).

We have argued here that the value of $R_{\text{in}} \sim 70 \text{ km}$ inferred from the *XMM-Newton* spectra is roughly representative of the true inner-disk radius (allowing for small correction factors). We have also shown that the fitted temperature increased with luminosity. The *Chandra* spectra were power-law-dominated but they also included a thermal component, and they were successfully fitted with a power-law plus disk-blackbody model; however, in that case, the characteristic radius R_c inferred from the disk-blackbody component was $R_c \sim 700\text{--}1000 \text{ km}$ (Soria et al. 2012), and the fitted temperature was lower, despite the higher luminosity. Our preferred explanation for this difference is that we are not measuring the same physical structure. In the *XMM-Newton* observations, taken near or just above the Eddington limit, the disk-like curvature of the spectrum and its high peak temperature ($kT \sim 1\text{--}2 \text{ keV}$) suggest that we are seeing emission directly from the inner region of the disk, close to the innermost stable circular orbit. In the *Chandra* observations, which we now recognize (by comparison with the *XMM-Newton* data) to correspond to higher accretion rates, the emission from the inner disk is completely Comptonized into a power-law, and the soft thermal excess corresponds to emission from larger disk radii, outside the hot Comptonizing region. This is consistent with its lower temperature ($kT \sim 0.2\text{--}0.4 \text{ keV}$) and lower relative contribution with respect to the power-law component. For power-law-dominated ULXs with a soft excess, it was suggested that the fitted radius of the thermal component may correspond to the spherization radius, so that $R_c \sim \dot{m} R_{\text{in}}$ (Soria 2007; Kajava & Poutanen 2009). This suggests that the *XMM-Newton* observations ($\dot{m} \sim 1$) reveal the true inner-disk radius, while the *Chandra* observations ($\dot{m} \sim 10$) give a characteristic ra-

dius an order of magnitude larger. Mis-identification of this larger characteristic radius in power-law-dominated ULXs as the innermost stable circular orbit led to speculations (now generally thought to be incorrect) that many ULXs could be intermediate-mass BHs with masses of a few $10^3 M_\odot$ (Miller et al. 2004; Soria 2007).

It is instructive to compare M 83 ULX-1 with M 33 X-8 (the brightest ULX in the Local Group), whose spectral properties and variability have been extensively studied with *XMM-Newton* (Middleton et al. 2011) and *Suzaku* (Isobe et al. 2012). The spectrum of M 33 X-8 displays a similar degree of curvature, and has been modelled either as slim disk or as a two-component inflow (warm, optically thick Comptonization medium in the inner region plus a cooler outer disk). The Comptonization model was preferred by Middleton et al. (2011) because the characteristic temperature of M 33 X-8 decreases with flux (contrary to the expectations for a slim disk) and a high-energy tails appears at the highest fluxes. In the *XMM-Newton* observations of M 83 ULX-1, instead, the characteristic temperature increases with flux (Table 2) and there is no hint of high-energy tails. Therefore, a slim-disk model is self consistent. For the *Chandra* spectra of M 83 ULX-1, the two-component Comptonization model provides the most physical explanation. In summary, as a rule of thumb, we interpret the curved spectrum of a ULX as disk emission when its fitted temperature increases with flux, and as Comptonization plus outer disk emission when its fitted temperature decreases with flux.

Sutton et al. (2013) have proposed a more refined three-state ULX classification, which distinguishes between “broadened disk”, “hard”, and “soft” ultraluminous spectra, roughly in order of increasing accretion rate and increasing optical depth of the outflows. Both the broadened-disk ($1 \lesssim \dot{m} \lesssim 10$) and the soft state (corresponding to the highest range of \dot{m}) appear curved, with a high-energy downturn, while the hard state is more power-law-like. In this picture, M 83 ULX-1 may have been in the broadened-disk regime (just above Eddington) during the *XMM-Newton* observations, and in the hard ultraluminous regime during the *Chandra* observations. In addition to the accretion rate, it is likely that other factors such as the viewing angle to the disk, wind geometry and hysteresis determine whether a ULX appears to us as a power-law or curved X-ray spectrum. Kawashima et al. (2012) have carried out hydrodynamic simulations which show how Comptonization and down-scattering in a thick outflow can provide a physical explanation for the evolution between power-law and curved ULX spectra as a function of accretion rate.

7. CONCLUSIONS

We used *XMM-Newton*, *Swift* and *Chandra* to follow the evolution of the transient ULX in M 83 that went into outburst sometime between late 2009 and 2010. Four years later, the outburst continues, and M 83 ULX-1 remains the most luminous point-like object in that galaxy, although not as bright as in 2011 February–March. After a temporary decline, during which X-1 dipped below the ULX threshold, it has now returned to an X-ray luminosity $\approx 2 \times 10^{39} \text{ erg s}^{-1}$.

Using high-quality *XMM-Newton* spectra from 2013–2014, we showed that M 83 ULX-1 has a curved spectrum, consistent with a slim disk regime, or more gen-

erally, with disk emission heavily modified by optically-thick Comptonization in a warm medium ($kT_e \lesssim 2$ keV). From the best-fitting model parameters in the three *XMM-Newton* epochs, we argue that the source is currently varying between the upper end of the high/soft state and a mildly super-Eddington (ultraluminous) state. Thus, the evolution of this source helps us understand the close relation between the most luminous Galactic BH binaries and ULXs.

From the best-fitting radius and temperature of the inner disk (in the framework of the slim-disk model), and from our argument that the source luminosity is varying within a factor of 2 of an Eddington luminosity $\approx 2 \times 10^{39}$ erg s $^{-1}$, we infer a BH mass ≈ 10 – $20 M_\odot$ (subject to uncertainties in the viewing angle and BH spin). This is consistent with the maximum mass of stellar BHs we expect to find in a metal-rich galaxy such as M83. It is a further argument in favour of the interpretation of most ULXs as super-critical accretors.

We plan to continue monitoring the outburst evolution of M83 ULX-1. If the outburst is declining, we will try to determine at what luminosities the system switches to the canonical high/soft state and then to the low/hard state, and therefore get a more accurate estimate of its BH mass and of its Eddington luminosity. If the outburst re-flares, we will test whether ULX-1 switches again to a power-law-dominated spectrum (as seen in the 2010–2011 *Chandra* observations) at higher luminosity.

We thank our additional colleagues on the companion multi-wavelength surveys of M83 for useful discussions. We thank the anonymous referee for useful suggestions that have improved our discussion. R.S. also thanks Chris Done, Hua Feng, Fabien Grisé, Matthew Middleton, Tim Roberts for useful discussions on ULX spectral states relevant to this work. Support for this work was provided by the National Aeronautics and Space Administration through Chandra grant No. GO1-12115, issued by the Chandra X-Ray Observatory Center, which is operated by the Smithsonian Astrophysical Observatory for and on behalf of NASA under contract NAS8-03060. R.S. acknowledges an Australian Research Council grant DP120102393. W.P.B. and K.K. acknowledge Chandra grant No. GO1-12115C to Johns Hopkins University. P.F.W. also acknowledges financial support from the National Science Foundation through grant AST-0908566.

REFERENCES

- Abe, Y., Fukazawa, Y., Kubota, A., Kasama, D., & Makishima, K. 2005, *PASJ*, 57, 629
- Arnaud, K. A. 1996, *Astronomical Data Analysis Software and Systems V* (ASP Conf. Ser. 101), ed. G. H. Jacoby & J. Barnes (San Francisco, CA: ASP), 17
- Belczynski, K., Bulik, T., Fryer, C. L., Ruiter, A., Valsecchi, F., Vink, J. S., & Hurley, J. R. 2010, *ApJ*, 714, 1217
- Blackburn, J. K. 1995, *Astronomical Data Analysis Software and Systems IV* (ASP Conf. Ser. 77), ed. R. A. Shaw, H. E. Payne, & J. J. E. Hayes (San Francisco, CA: ASP), 367
- Bresolin, F., & Kennicutt, R. C. 2002, *ApJ*, 572, 838
- Castro-Tirado, A. J., Brandt, S., Lund, N., Lapshov, I., Sunyaev, R. A., Shlyapnikov, A. A., Guziy, S., & Pavlenko, E. P. 1994, *ApJS*, 92, 469
- Davis, S. W., Blaes, O. M., Hubeny, I., & Turner, N. J. 2005, *ApJ*, 621, 372
- Done, C., & Kubota, A. 2006, *MNRAS*, 371, 1216
- Fender, R. P., Belloni, T. M., & Gallo, E. 2004, *MNRAS*, 355, 1105
- Feng, H., & Soria, R. 2011, *NewA Rev.*, 55, 166
- Frank, J., King, A. R., & Raine, D. J. 2002, *Accretion Power in Astrophysics* (Cambridge: Cambridge University Press)
- Fruscione, A., McDowell, J. C., Allen, G. E., et al. 2006, *Proc. SPIE*, 6270, 62701V
- Gierliński, M., Done, C., & Page, K. 2009, *MNRAS*, 392, 1106
- Gladstone, J. C., Roberts, T. P., & Done, C. 2009, *MNRAS*, 397, 1836
- Isoe, N., Kubota, A., Sato, H., & Mizuno, T. 2012, *PASJ*, 64, 119
- Kajava, J. J. E., & Poutanen, J. 2009, *MNRAS*, 398, 1450
- Kawaguchi, T. 2003, *ApJ*, 593, 69
- Kawashima, T., Ohsuga, K., Mineshige, S., Yoshida, T., Heinzeller, D., & Matsumoto, R. 2012, *ApJ*, 752, 18
- King, A. R. 2014, *Science*, 343, 1318
- Kreidberg, L., Bailyn, C. D., Farr, W. M., & Kalogera, V. 2012, *ApJ*, 757, 36
- Kubota, A., & Makishima, K. 2004, *ApJ*, 601, 428
- Kubota, A., Mizuno, T., Makishima, K., Fukazawa, Y., Kotoku, J., Ohnishi, T., & Tashiro, M. 2001, *ApJ*, 547, L119
- Kubota, A., Tanaka, Y., Makishima, K., Ueda, Y., Dotani, T., Inoue, H., & Yamaoka, K. 1998, *PASJ*, 50, 667
- Kulkarni, A. K., et al. 2011, *MNRAS*, 414, 1183
- Liu, J.-F., Bregman, J. N., Bai, Y., Justham, S., & Crowther, P. 2013, *Nature*, 503, 500
- Long, K. S., Kuntz, K. D., Blair, W. P., Godfrey, L., Plucinsky, P. P., Soria, R., Stockdale, C., & Winkler, P. F. 2014, *ApJS*, 212, 21
- McClintock, J. E., & Remillard, R. A. 2006, *Black Hole Binaries*, ed. W. H. G. Lewin & M. van der Klis (Cambridge: Cambridge Univ. Press), 157
- Makishima, K. 2007, *IAUS*, 238, 209
- Makishima, K., Maejima, Y., Mitsuda, K., Bradt, H. V., Remillard, R. A., Tuohy, I. R., Hoshi, R., & Nakagawa, M. 1986, *ApJ*, 308, 635
- Makishima, K., et al. 2000, *ApJ*, 535, 632
- Middleton, M. J., Sutton, A. D., & Roberts, T. P. 2011, *MNRAS*, 417, 464
- Miller, J. M., Fabian, A. C., & Miller, M. C. 2004, *ApJ*, 614, L117
- Mitsuda, K., et al. 1984, *PASJ*, 36, 741
- Mizuno, T., Kubota, A., & Makishima, K. 2001, *ApJ*, 554, 1282
- Motch, C., Pakull, M. W., Soria, R., Grisé, F., & Pietrzyński, G. 2014, *Nature*, 514, 198
- Pilyugin, L. S., Thuan, T. X., & Vilchez, J. M. 2006, *MNRAS*, 367, 1139
- Pilyugin, L. S., Vilchez, J. M., & Thuan, T. X. 2010, *ApJ*, 720, 1738
- Poutanen, J., Lipunova, G., Fabrika, S., Butkevich, A. G., & Abolmasov, P. 2007, *MNRAS*, 377, 1187
- Roberts, T. P. 2007, *Ap&SS*, 311, 203
- Saha, A., Thim, F., Tammann, G. A., Reindl, B., & Sandage, A. 2006, *ApJS*, 165, 108
- Shakura, N. I., & Sunyaev, R. A. 1973, *A&A*, 24, 337
- Shimura, T., & Takahara, F. 1995, *ApJ*, 445, 780
- Shrader, C. R., & Titarchuk, L. 2003, *ApJ*, 598, 168
- Sobczak, G. J., McClintock, J. E., Remillard, R. A., Bailyn, C. D., & Orosz, J. A. 1999, *ApJ*, 520, 776
- Sobczak, G. J., McClintock, J. E., Remillard, R. A., Cui, W., Levine, A. M., Morgan, E. H., Orosz, J. A., & Bailyn, C. D. 2000, *ApJ*, 531, 537
- Soria, R. 2007, *Ap&SS*, 311, 213
- Soria, R. 2011, *AN*, 332, 330
- Soria, R., Kuntz, K. D., Winkler, P. F., Blair, W. P., Long, K. S., Plucinsky, P. P., & Whitmore, B. C. 2012, *ApJ*, 750, 152
- Soria, R., Long, K. S., Blair, W. P., Godfrey, L., Kuntz, K. D., Lenc, E., Stockdale, C., & Winkler, P. F. 2014, *Science*, 343, 1330
- Steiner, J. F., McClintock, J. E., Remillard, R. A., Gou, L., Yamada, S., & Narayan, R. 2010, *ApJ*, 718, L117
- Stobbart, A.-M., Roberts, T. P., & Wilms, J. 2006, *MNRAS*, 368, 397
- Sutton, A. D., Done, C., & Roberts, T. P. 2014, *MNRAS*, 444, 2415

- Sutton, A. D., Roberts, T. P., & Middleton, M. J. 2013, MNRAS, 435, 1758
- Thorne, K. S. 1974, ApJ, 191, 507
- Tomsick, J. A., Corbel, S., Goldwurm, A., & Kaaret, P. 2005, ApJ, 630, 413
- Vierdayanti, K., Watarai, K., & Mineshige, S. 2008, PASJ, 60, 653
- Watarai, K., Fukue, J., & Mineshige, S. 2000, PASJ, 52, 133
- Watarai, K., & Mineshige, S. 2003, ApJ, 596, 421
- Watarai, K., Mizuno, T., & Mineshige, S. 2001, ApJ, 549, L77